Structural characterization of SLYM - a 4th meningeal membrane

Virginia Plá[1], Styliani Bitsika[1], Michael Giannetto[2], Antonio Ladron-de-Guevara[2], Daniel Gahn-Martinez[2], Yuki Mori[1], Maiken Nedergaard[1,2*] and Kjeld Møllgård[3*]

1: Division of Glial Disease and Therapeutics, Center for Translational Neuromedicine, Faculty of Health and Medical Sciences, University of Copenhagen, 2200 Copenhagen, Denmark.

2: Division of Glial Disease and Therapeutics, Center for Translational Neuromedicine, University of Rochester Medical Center, Rochester, NY 14642, USA.

3: Department of Cellular and Molecular Medicine, Faculty of Health and Medical Sciences, University of Copenhagen, 2200 Copenhagen, Denmark.

*: Corresponding authors

MN: nedergaard@urmc.rochester.edu

KM: kjm@sund.ku.dk

Abstract

Traditionally, the meninges are described as 3 distinct layers, dura, arachnoid and pia. Yet, the classification of the connective meningeal membranes surrounding the brain is based on postmortem macroscopic examination. Ultrastructural and single cell transcriptome analyses have documented that the 3 meningeal layers can be subdivided into several distinct layers based on cellular characteristics. We here re-examined the existence of a 4th meningeal membrane, Subarachnoid Lymphatic-like Membrane or SLYM in Prox1-eGFP reporter mice. Imaging of freshly resected whole brains showed that SLYM covers the entire brain and brain

stem and forms a roof shielding the subarachnoid cerebrospinal fluid (CSF)-filled cisterns and the pia-adjacent vasculature. Thus, SLYM is strategically positioned to facilitate periarterial influx of freshly produced CSF and thereby support unidirectional glymphatic CSF transport. Histological analysis showed that, in spinal cord and parts of dorsal cortex, SLYM fused with the arachnoid barrier layer, while in the basal brain stem typically formed a 1-3 cell layered membrane subdividing the subarachnoid space into two compartments. However, great care should be taken when interpreting the organization of the delicate leptomeningeal membranes in tissue sections. We show that hyperosmotic fixatives dehydrate the tissue with the risk of shrinkage and dislocation of these fragile membranes in postmortem preparations.

Keywords

Cerebrospinal fluid, perivascular space, glymphatics, Prospero Homeobox 1, Neuroimmune.

49 *Introduction*

50 Numerous studies have over the past decade shown that glymphatic fluid flow removes
51 amyloid-β and other waste products of neural metabolism from brain parenchyma (1). These
52 findings, along with the discovery of the meningeal lymphatic vessels, have sparked a new
53 interest in brain fluid transport (2). Parallel investigations documented that
54 glymphatic/lymphatic clearance is suppressed in aging and that the decline in brain fluid
55 transport is accentuated in patients suffering from neurodegenerative diseases compared
56 with age-matched non-demented control subjects (3-7). An emerging question is whether
57 therapies that restore glymphatic/lymphatic clearance can delay the onset of dementing
58 diseases or modify their progression (8).

59 One aspect of brain fluid transport that has received little attention is the functional
60 organization of the large CSF-filled subarachnoid space (SAS) surrounding the brain. SAS is
61 logically central for the organization of brain fluid transport, yet essentially no information
62 exists on CSF dynamics in the SAS. Most data regarding the structure of SAS is based on
63 histological analysis. Postmortem histological analysis of the SAS poses a potential problem
64 since death and formaldehyde-based fixation eliminate the fluid filled spaces in both
65 peripheral tissues (9) and brain (10, 11). We recently described the existence of a 4th
66 meningeal membrane, the Subarachnoid Lymphatic-like Membrane, SLYM, surrounding the
67 mouse and human brain (12). SLYM was identified by the expression of Prospero Homeobox
68 1 (Prox1), which is a transcription factor that drives lymphatic endothelial fate (13).
69 Consequently, Prox1-eGFP reporter mice are often used along with other lymphatic markers
70 to identify lymphatic or lymphatic-like tissues (14). Structurally, SLYM is composed of a single
71 cell layer that only expresses a subset of lymphatic markers, Prox1 and podoplanin, but not
72 VEGFRC or LYVE1 (15). SLYM is therefore best characterized as a lymphatic-like meningeal

73 layer. Structurally and phenotypically, SLYM was shown to differ from the 3 traditional
74 meningeal membranes—including dura, the arachnoid barrier cell (ABC) layer, and pia—as
75 well as from the arachnoid trabecula and lymphatic vessels (12). Functional in vivo analysis
76 showed that SLYM compartmentalizes the SAS into two separate CSF pools (12), thus directing
77 CSF transport in the SAS.
78 CSF is, at least in part, produced by the choroid plexus and exits the ventricles via the foramen
79 of Magendie and Luschka (16). From here, the freshly produced CSF enters the basal cisterns,
80 initially flowing into the cisterna magna, which is continuous with the interpeduncular cistern
81 surrounding the circle of Willis. The interpeduncular cistern serves as a pool of CSF that is
82 transported up along the perivascular space surrounding the 3 major cerebral arteries, the
83 anterior, middle and posterior cerebral arteries in both rodents and human brain (1, 17). We
84 showed that SLYM creates a roof over the pia-adjacent arteries as they follow the brain
85 surface, thus facilitating that the freshly produced CSF in the basal cisterns is transported
86 along the 3 major cerebral vessels (anterior, middle and posterior) rather than mixing with
87 CSF in the larger SAS. However, online comments raised criticism of our description of SLYM**.**
88 One set of critiques stated that our finding contradicted prior histological studies showing that
89 SAS is a single large compartment. Another point of critique was that the immunolabeling
90 analysis did not sufficiently document the ABC layer and SLYM as separate layers. The last set
91 of critiques stated that our *in vivo* tracer injection failed to document the existence of 2
92 distinct SAS compartments. It was suggested that the injections created an artificial space and
93 that one of the CSF-filled compartments was the subdural space. The subdural space —which
94 does not exist during physiological conditions— is a compartment created by an intradural
95 separation between the dura *per se* and the dural border layer. Yet, the same authors' recent
96 studies dissecting the meningeal layers provided histological and single cell transcriptome

97 evidence for the existence of a Prox1-positive meningeal layer located below the ABC layer
98 (18, 19), as we originally reported (12). In vivo studies also confirmed that SLYM and dura are
99 separated by a CSF-filled compartment, but the authors concluded that it was an artificial
100 space without explanation. Based on the histological and transcriptome analysis, the SLYM
101 layer was labeled BFB2-3 (18, 19).
102 In this report, we have extended the characterization of SLYM and confirmed that SLYM is
103 indeed a distinct membrane that surrounds the entire brain. More specifically, SLYM forms a
104 roof covering the CSF-filled cisterns and pial perivascular spaces creating a continuous CSF-
105 filled compartment. We provide evidence showing that SLYM immunophenotypically differs
106 from the ABC layer and a critical literature review documents that compartmentalization of
107 SAS, by either a single- or double-layered membrane, has been reported earlier (20, 21). In
108 the older literature, SLYM has been described as the inner or reticular arachnoid membrane.
109 We conclude that SLYM *in vivo* represents a distinct meningeal membrane that can fuse during
110 fixation with the ABC layer or the pial membrane depending on the location. However, in the
111 basal part of the brain SLYM creates two separate CSF-containing SAS compartments, even
112 seen in paraffin sections. We speculate that this arrangement facilitates that fresh CSF
113 produced in the ventricles is guided directly up along the cerebral arteries instead of being
114 mixed with the larger pool of CSF surrounding the brain.
115
116 *Results*
117 Fixation-induced shrinkage of the brain
118 In the classical electron microscopy (EM) literature, SLYM is recognized as the inner arachnoid
119 layer or the reticular layer of the arachnoid membrane. SLYM will in EM typically adhere to
120 the ABC layer. Could the cohesion be an artificial product of displacement of the fragile

121 meningeal membrane when preparing histological samples? To illustrate the significant
122 shrinkage of the brain and the expansion of the subarachnoid space upon perfusion fixation,
123 we first visualized the live and dead mouse brain *in situ* by high field magnetic resonance
124 imaging (MRI) (**Fig. 1A**). The MR imaging clearly illustrates that, in a live young mouse, the
125 brain fills most of the cranial cavity; and how small a volume the subarachnoid space
126 surrounding the brain surfaces occupies. After death, the brain expands but swelling is
127 restricted by the skull, resulting in compression of the subarachnoid and ventricular spaces
128 (**Fig. 1A**). Our previous studies have documented that influx of CSF via the glymphatic system
129 accounts for most of the acute edema formation after cardiac arrest (22). In sharp contrast,
130 the perfusion-fixated brain imaged in thin paraffin sections exhibited a significant degree of
131 shrinkage resulting in displacement of the brain within the skull cavity (**Fig. 1B-C**). The
132 properties of skull's bony structure do not change when exposed to fixative, in contrast to the
133 soft tissue including the brain and the meningeal membranes. The striking reduction in brain
134 volume during histological preparation results in the creation of large empty spaces
135 surrounding the brain in the perfusion-fixated brain (9, 11). It appears that the membranes
136 fuse to different surfaces during perfusion-fixation, with the ABC layer localized to the skull
137 (stained for Cld-11, Fig. 1D, top), and the SLYM localized to the brain surface (stained for GFP,
138 Fig1D, bottom). This further suggests the SLYM membrane is not always fused with the ABC
139 layer and we conclude that the fragile leptomeningeal membranes are prone to displacement
140 and fixation artifacts in histological sections.

141 <u>SLYM creates a unique CSF compartment encompassing the cisterns and pial perivascular</u>
142 <u>spaces</u>

143 To interrogate the functional significance of SLYM covering the brain, Prox1-eGFP mice were
144 injected with either a small size tracer (Evans Blue, 0.9 kDa) or a larger tracer—Bovine Serum

145 Albumin—coupled to a fluorophore (BSA-Alexa Fluor 647, 67 kDa). The tracers were injected
146 via a cannula placed in the cisterna magna and allowed to circulate for 30 min in anesthetized
147 mice (ketamine/xylazine, K/X) before harvest (**Fig. 2A**). CSF tracers delivered by this procedure
148 are initially transported into the basal cisterns followed by an influx along the perivascular
149 space surrounding the large cerebral arteries and driven by arterial pulsations (10). The mice
150 were intracardially perfused with phosphate-buffered saline (PBS) to eliminate any signal from
151 the vascular compartment. First, the unfixed brains were rapidly extracted and imaged using
152 a fluorescent macroscope to avoid fixation artifacts (**Fig. 2B-C and Sup. Figs. 1 and 2**) (11).
153 Macroscopic imaging of the intact whole brains allowed the visualization of Evans Blue and
154 BSA-647 confined within the inner CSF-filled SAS compartment below the SLYM layer. Visual
155 inspection revealed that both the small and large tracers were confined within the cisterns
156 including cisterna magna, the pontine cistern, the interpeduncular cistern, the
157 cerebellopontine angle cistern, and several other minor cisterns. The perivascular spaces
158 surrounding the anterior, middle, and posterior cerebral arteries were also clearly delineated
159 by both CSF tracers (**Fig. 2B-C and Sup. Fig. 1B**). Close-up images showed the perivascular
160 location of the tracer and Prox1-eGFP+ cells covering the tracer-filled periarterial spaces
161 creating one continuous, closed CSF-filled SAS compartment (**Fig. 2C**). High-magnification
162 images were combined with whole-mount confocal and two-photon imaging to further
163 investigate whether the tracers were contained below the SLYM layer. When extracting the
164 brains from Prox1-eGFP reporter mice, we noted that SLYM adheres to the surface of the brain
165 rather than to dura, which stays attached to the skull (**Fig. 2D**) (23). In contrast, the ABC layer
166 detected in the fixed skull immunolabeled positive for dipeptidyl peptidase IV (DPP4). an
167 enzyme suggested to participate in neuropeptide metabolism at the outer arachnoid, adhered

168 to dura (**Fig. 2D**) (19). These observations show that SLYM creates a unique CSF compartment
169 encompassing the cisterns and the pial perivascular spaces.

170 <u>High resolution immunohistochemical characterization of SLYM</u>

171 The first description of SLYM (12) included a detailed immunohistochemical characterization
172 of the newly discovered meningeal layer surrounding the mouse and human brain. To further
173 characterize SLYM, whole heads along with the attached upper cervical region harvested from
174 Prox1-eGFP mice were decalcified. Decalcification is the only approach that allows the
175 preparation of thin paraffin sections, containing all the meningeal layers located between the
176 parenchyma and the surrounding skull or vertebrae. Bright field immunohistochemistry based
177 on horseradish peroxidase staining (HPS) was utilized rather than fluorescence labeling to
178 ensure optimal sensitivity and specificity of the antibody labeling. Consecutive sections were
179 used when comparing the pattern of labeling of multiple antibodies to avoid double labeling
180 of the thin membranes (**Fig. 3-7**).

181 eGFP immunolabelling was first employed to identify the exact anatomical location of SLYM in
182 sagittal sections in PROX1-eGFP reporter mice (**Fig. 3**). The analysis showed that SLYM forms
183 a meningeal layer encasing the entire brain, including the ventral and dorsal brain surfaces
184 (**Fig. 3A**). Higher power micrographs of the sagittal section document that SLYM forms a roof
185 covering the rostral basal cisterns (**Fig. 3B**), the more caudal cisterna pontis (**Fig. 3C**), and
186 dorsally delineates cisterna tegmentalis (also named cisterna superior), as indicated by
187 arrowheads (**Fig. 3E**), and the superior cerebellar cistern (**Fig. 3F**). Note that the slender and
188 more delicate SLYM membrane covering the superior surface of cerebellum deviates from
189 attachment to the skull (two right arrowheads pointing upwards) to approach the cerebellar
190 pial surface (three left arrowheads pointing downwards). The somewhat thicker appearing
191 SLYM of the cisterna pontis (**Fig. 3C**), part of which is shown in higher magnification in **Fig. 3D,**

192 consists of two layers – the one-layered SLYM *per se* adjoined by an outer unstained cell layer
193 (arrowheads).
194 We next ask whether Prox1-eGFP+ SLYM cells in certain regions merged to form a double
195 membrane with the ABC layer. For this analysis, the well-characterized marker for the ABC
196 layer, an antibody directed against the tight junction protein Claudin-11 (24), was used in
197 combination with CRABP2 that labels SLYM (12, 15). Upon examining the relationship between
198 the two membranes, it became evident that SLYM and ABC layers are fused below foramen
199 magnum, and together form a double membrane adjoining dura, i.e., spinal meninges that
200 covers the cavity of the upper spinal canal (**Fig. 4A**). However, rostral to the foramen magnum,
201 corresponding to cranial meninges, SLYM and ABC layers separate: the ABC layer is located in
202 close proximity to dura, while SLYM continues as solitary membrane subdividing the
203 subarachnoid space (SAS) into an inner and outer CSF-filled compartment at the base of the
204 brain (**Fig. 4B**). Inner and outer subarachnoid spaces are obvious at the mid-pontine level (**Fig.**
205 **4C-D**).
206 High magnification imaging of SLYM around the basilar artery (**Fig. 5A-C**) provided additional
207 evidence for compartmentalization of the SAS by SLYM. Serial sections prepared from a Prox1-
208 eGFP reporter mouse were reacted with multiple antibodies, including eGFP, Prox1 (note the
209 nuclear labeling – arrowheads in **Fig. 5B**), and ER TR7, which also labeled the adventitia of the
210 artery (**Fig. 5C**). SLYM from cisterna ambiens (**Fig. 5D**) is closely attached to the ABC layer
211 (arrowheads), but is also coherent with an unstained layer of arachnoid reticular cells facing
212 the inner subarachnoid space (thin, open arrows).
213 Immunostaining of coronal sections against eGFP prepared from a Prox1-eGFP reporter
214 mouse depicted again that SLYM forms a complete membrane that covers the basal cisterns
215 (here cisterna pontis (CiP)) and is separated from the ABC layer (**Fig. 6**). SLYM seems to fuse

216 with pia along the basolateral pons, thus creating separated inner SAS spaces – one median
217 and two lateral (see arrows in **Fig. 6**). The wall of the lateral cisterna ambiens (CiA) is always
218 thick and strongly stained.
219 Additional immunostaining showed that SLYM also fuses with pia along the medial and lateral
220 borders of the cisterna caroticus (CiC) (arrows in **Fig. 7A**). This figure which is stained for
221 claudin-11 demonstrates that SLYM is distinct from and not stained by anti-claudin 11**. Fig. 7B-**
222 **I** depict SLYM covered by inner and outer layers of fibroblasts characterized by several
223 different antigens. The detailed analysis of serial sections documented that SLYM *per se* is
224 negative for claudin-11 and does not stain positive for E-Cadherin or LYVE1. However, SLYM
225 and associated fibroblast layers exhibited positive immunolabeling for PDPN, ER TR7, RALDH2,
226 plectin and Prox1. Additionally, the analysis showed that SLYM hosts several LYVE-1
227 immunopositive macrophages (**Fig. 7F**).
228 In our fixed histology material, we have encountered the one-layered SLYM membrane as an
229 entity by itself (**Fig. 4**), as well as SLYM covered by or covering another layer of leptomeningeal
230 fibroblasts, thus appearing as a part of a two-layered structure (**Fig. 3D**) as our previously
231 demonstrated ABC/SLYM layers. In certain sub-regions of the basal cisterns, SLYM appears to
232 be 'sandwiched' between both an inner and an outer lepto–meningeal fibroblast layer (**Fig.**
233 **7**). The presence of 'sandwiched SLYM' in the basal cisterns raises the possibility that extra
234 leptomeningeal layers are required to support and reinforce SLYM in this region due to the
235 heavy pulsations from the large basilar arteries.
236 <u>Comparing new data with the classical literature</u>
237 Has a meningeal membrane matching SLYM been described in the classical literature? To
238 interrogate previously published data, we reproduced the toluidine blue-stained semithin
239 section-based scheme of Orlin et al. in 1991 (21). In fact, the Orlin publication reproduced the

classical sketch from Nabeshima et al. in 1975 to frame their own data into a historical context (20). We have here color-coded the panels from both publications to compare the meningeal layers in these publications to the data reported here (**Fig. 8A-B**). The Nabeshima scheme, as well as the Orlin semithin section, depicts a mono-cell layer (green) between the arachnoid and the pial cell layers (both gray) that covers a pia-adjacent vessel (red). We propose that the green-colored membranes in **Fig. 8A-B** represent SLYM, as these membranes rest on the pia-adjacent vasculature and the cytosol of the cells is translucent. The panels depict the green membrane as separating the SAS into two compartments and clearly illustrate that this subdivision of SAS differs from the artificial subdural space between dura and the ABCL in the Nabeshima scheme. For comparison, an orthogonal view of a pia-adjacent blood vessel containing CSF tracer in the perivascular space from our analysis is included (**Fig. 8C**). A graphical scheme is included on top to illustrate that the SLYM layer defines the pial perivascular space by creating a roof resting on top of the pia-adjacent vasculature (**Fig. 8C**).

Discussion

The meninges surrounding the brain are classically identified as dura, arachnoid and pia. The meningeal layers are all composed of connective tissue and their designation is based on macroscopic postmortem examination. The simplified classification of the meningeal membranes into 3 layers was questioned already in the first detailed histological studies of the meninges (20, 21). We recently described a 4th meningeal membrane, SLYM (Sub-arachnoid Lymphatic-like Membrane), in both mouse and human brains (12). SLYM is located within the subarachnoid space (SAS), the large CSF-filled spaces that surround the brain, between the arachnoid and pia (12). We here reexamined the structural characteristics of SLYM. We confirmed that SLYM surrounds the entire brain and, based on immunolabeling,

264 demonstrated that SLYM phenotypically differs from the arachnoid barrier cell (ABC) and pia
265 layers (**Figs. 2-6**). Our findings revealed that SLYM rests on top of the pia-adjacent vasculature,
266 forming a roof over the cisterns and the pia-adjacent vasculature. As such, SLYM creates a
267 continuous CSF-filled space encompassing the cisterns and the pial perivascular spaces. The
268 unique position of SLYM becomes particularly evident after extracting the brain in Prox1-eGFP
269 reporter mice wherein a CSF tracer circulated for 30 min. Macroscopic imaging of freshly
270 resected brains showed that SLYM retains the CSF tracers within the cisterns and the pial
271 perivascular spaces, outlining a large tracer-filled space that limits the spread of both a small
272 and a large CSF tracer. When dissecting the brains of Prox1-eGFP reporter mice, we observed
273 that SLYM preferentially adheres to the brain's surface rather than to the dura, which remains
274 firmly attached to the skull. Conversely, the ABC layer, marked by positive DPP4
275 immunolabeling, exhibits a distinct adherence to the dura and skull. Similar separation
276 between SLYM and the ABC layer is also evident in decalcified, paraffin-embedded sections
277 (**Fig. 1**). Hence, these observations confirm that SLYM divides the larger subarachnoid space
278 into two separate compartments (**Fig. 2**).
279 The subarachnoid space (SAS) is in most textbooks depicted as a single compartment.
280 However, Liliequist (25) described already in 1956 a compartmentalization of the SAS. He
281 described a '*thin arachnoid membrane*', considering this layer as '*the line of demarcation*
282 *between the chiasmatic and the intercrural cisterns, possessing as it does the advantages of a*
283 *definite anatomic structure*'. This membrane, which has become an essential intraoperative
284 landmark named after its discoverer (26), is one of the better-known subdivisions of the SAS,
285 but not the only one (27).
286

287 In the past, special attention has been given to the ABC layer, often described as a single
288 barrier membrane that isolates the brain from the entrance of exogenous substances.
289 Brøchner et al., 2015 (24) identified claudin 11 as the tight junction protein responsible for
290 the barrier function of the ABC layer. However, multiple studies have documented that the
291 ABC layer is more complicated, consisting of multiple cell types based on their ultrastructural
292 features. In 1974, Lopes and Mair (28) summarized in their publication an analysis of the
293 meningeal membrane in diverse animals and concluded that the arachnoid membrane is
294 formed by at least two layers of cells, the outermost of them being electron dense with tight
295 junctions and accompanied by an inner layer of clear cells occasionally separated by spaces
296 and surrounded by loose collagen fibers. A basement membrane was noted to separate the
297 superficial dark cells from the inner layer of the arachnoid membrane. In addition, dense cells
298 with features of fibroblast could be found along the collagen fibers of the inner layer of clear
299 cells (28). Nabeshima et al. 1975 conducted an electron microscopy (EM) and freeze-
300 fracturing study, which was also based on analysis of multiple species. This publication also
301 concluded that the ABC layer differs from the inner arachnoid cells with lighter cytosol (20).
302 Moreover, Nabeshima et al, stated that: "*The cells of the pia were similar to the arachnoid*
303 *cells but their processes were somewhat thinner. We were unable to find any cytological*
304 *criteria for differentiating these cells from the layer of arachnoid cells next to the pia and,*
305 *therefore, consider this inner layer of arachnoid and the pia to be basically one layer in which*
306 *the different shapes of the cells are determined by the shapes of the structures they invest".*
307 This note highlights the fact that the classification of the 3 connective tissue meningeal
308 membranes, dura, arachnoid and pia is based on macroscopic examination and that the inner
309 arachnoid and the outer pial layers in histological sections do not exhibit distinct
310 characteristics. The Nabeshima publication included a schematic of the meningeal layers, in

311 which only features common to all the specimens of animals studied were included (20). This
312 schematic was later used by Orlin et al. in 1991 (21) to illustrate the similarities between their
313 own findings to those of Nabeshima et al. (20). We have here reproduced the figure from the
314 Orlin et al publication along with data from our own study to highlight the similarities between
315 the 3 reports (**Fig. 8**).
316 In 1983 - 84, Krisch, Leonhardt and Oksche's work (29, 30) moved the field forward by studying
317 the functional role of this meningeal segmentation through the injection of horseradish
318 peroxidase (HRP) in different regions of the brain and meninges. They described that HRP
319 distributed within at least 2 separate compartments of the SAS, which they entitled the
320 arachnoid or pial spaces. The authors also defined the '*intermediate lamella*', a structure
321 composed by the inner arachnoid layer and the outer pial membrane, that dissociates when
322 joining a blood vessel bridging in between the dura to the pia-adjacent vasculature. The
323 intermediate lamella here forms a perivascular space surrounding the bridging vessel (30).
324 HRP injected into either the arachnoid or pial spaces demonstrated that the intermediate
325 lamella is indeed a barrier that separates the CSF-filled arachnoid and pial compartments, as
326 we later described (12). The same technique was used by Orlin et al. 1991 (21), who infused
327 HRP-mixed blood to mimic acute subdural hemorrhages. Their detailed electron microscopy
328 analysis led to the description of the arachnoid reticular cells, as '*a 10-20 µm thick layer*
329 *composed of irregularly branched cells'*. Adhering junctions were noted scattered both
330 between the arachnoid reticular light cells and between these and the barrier cells (21). Later,
331 Vandenabeele, Creemers and Lambrichts 1996 (31) described the '*arachnoid border cells*' as
332 sinuous flattened cells found along the inner surface of the arachnoid reticular layer, with
333 uncertain nature, that could belong to either the arachnoid or pial layer. Several investigators
334 have noted that the cytoarchitecture of these cells is so similar that the cells cannot be

335 designated as belonging to either the inner arachnoid or outer pia cell layers based on their
336 cellular characteristics.
337 Recently, Pietilä et al., 2023 confirmed the presence of a Prox1+ cell layer below the ABC layer
338 (19). Electron microscopy and transcriptome analysis added additional support to the
339 presence of a distinct Prox1+ cell layer which cells were coupled by adherence junctions
340 composed of ve-Cadherin (CDH5) and gap junctions, Cx43, Cx30 and Cx26 (Gja1, Gjb6 and
341 Gjb2). The authors documented that a Prox1-tdTomato+ layer is located below the ABC layer.
342 A publication by the same groups interrogated the location of SLYM in relationship to the ABC
343 layer and pia (18). *In vivo* analysis showed that SLYM (Prox1-tdTomato+/ve-Cadherin-GFP) is
344 separated from dura by a CSF-filled space in cortex (Figs. 1L and 6F). However, the authors
345 concluded that the CSF-filled space was artificial and created during surgery or injections. This
346 conclusion was based on the evidence that depicts the meningeal layers adhere to each other
347 in histological sections, and the observation that the depth of CSF-filled space appears to
348 enlarge during imaging and depends upon the surgery (18). One problem with the *in vivo*
349 experiments was the use of ve-Cadherin reporter mice that are not specific to any of the
350 meningeal layers. In the ve-Cadherin-eGFP reporter mice, a subpopulation of cells located in
351 both dura and the ABC layer express GFP, as well as most cells in SLYM and pia. Thus, the GFP
352 signal functions as a pan-meningeal label and it is not possible to separate the distinct
353 meningeal layers *in vivo*. This conclusion is supported by the single cell transcriptome analysis
354 showing that dural border cells, ABC layer, SLYM (Prox1-positive cells named BFB2 and 3) and
355 pial cells all express ve-Cadherin (19).
356 We have in this study used markers that are only expressed by either the ABC layer or by
357 SLYM. That enabled us to demonstrate, both in the freshly resected brain (**Fig. 2**) and *ex vivo*
358 (**Figs. 3-7**), that the subarachnoid space is subdivided into two separate compartments by

359 SLYM. SLYM acts as a barrier for a CSF small tracer (Evans blue, 1 kDa), a slightly larger tracer
360 (TMR-conjugated dextran, 3 kDa), a large tracer (or BSA-647, 67 kDa) and 1 µm microspheres
361 (**Fig. 2**) (12). It is here important to note that the literature is based on postmortem histological
362 analysis, which results in major displacement of the CNS structures (11). The MR imaging of
363 the live brain *in situ* when compared with paraffin sections of whole head provided direct
364 evidence for major restructuring of the SAS due to the shrinkage of the soft tissue (brain,
365 meningeal membranes, vasculature and more), while the structural properties of bony skull
366 do not notably change (**Fig. 1**). We propose that the fragile SLYM layer located in the SAS is
367 displaced during the specimen preparation. In histological sections, SLYM seems to adhere to
368 either the ABC layer or pia, depending on where the fixative first reaches the tissue and
369 induces shrinkage of the subarachnoid space and deformation of the leptomeningeal
370 membranes.
371 In general, SLYM appears as a single, thin cell layer that often seems to fuse with the E-
372 Cadherin positive ABC layer membrane over dorsal cerebral cortex in histological sections, as
373 documented in Møllgård et al. (Fig. 4C-D in ref (12)) and originally described by Orlin et al. in
374 the spinal cord (21). A similar appearance is present at the cerebellar surface. In the caudal
375 cisternal system, SLYM is a part of a two-layered membrane covered towards the inside by a
376 collagen-VI containing fibroblast layer. Around the rostral basal cisterns, however, SLYM is
377 'sandwiched' between an inner and an outer fibroblast layer creating a thick 3-layered
378 membrane clearly separated from the ABC layer (**Fig. 7**). RALDH2 exemplifies the inner layer
379 and plectin the outer. The reinforcement/strengthening of SLYM covering the cisterns
380 containing the large intracranial arteries might reflect that arterial pulsatility in these cisterns
381 drives fresh CSF from the ventricles up along the anterior, middle, and posterior cerebral

382 arteries. At the transition between the skull and the vertebrae, SLYM appears to fuse with the
383 ABC layer (**Fig. 3**)
384 As discussed, the best separation of SLYM and the ABC layer was noted at the base of the
385 brain. SLYM here serves the important function of separating the subarachnoid space into two
386 CSF-filled compartments facilitating the transport of newly produced CSF along the
387 perivascular spaces. Loss of the SLYM barrier function here may be expected to disrupt the
388 unidirectional glymphatic transport of CSF, with the result that CSF containing amyloid, tau,
389 synuclein and other waste products is recirculated back into the brain. The resultant inflow of
390 aggregation-prone peptides and proteins may contribute to both the initiation and
391 progression of proteinopathic neurodegenerative diseases. Future studies dissecting key
392 questions, such as the age-related atrophy of SLYM, or its role in neuroinflammation, will be
393 necessarily imprecise in the absence of a designated name for the SLYM membrane. The
394 existing names for SLYM include the inner arachnoid layer, the reticular layer of the arachnoid
395 membrane, and latest, BFB2-3. We propose that the name SLYM, used to specify a distinct
396 meningeal membrane, will help to ensure the precision and replicability of future studies – in
397 an unnecessarily contentious field.
398
399 *Materials and Methods*
400 Animals
401 Both wildtype C57BL/6JRj and Prox1-EGFP+ (Janvier Labs, Le Genest-Saint-Isle, France) (14)
402 female and male mice were utilized at postnatal age 90-120 days. Mice were housed in groups,
403 containing 4-5 mice per cage, with controlled humidity and temperature, 12 hours light-dark
404 cycle (6:00 AM/6:00 PM) and regular access to tap water and chow food ad libitum. All
405 experiments carried out at the University of Copenhagen were approved by the Animal

406 Experiments Council under the Danish Ministry of Environment and Food (license number:
407 2015-15-0201-00535) and the procedures were performed in accordance with the European
408 directive 2010/63/EU, with every effort undertaken to reduce the utilization of animals.
409 Experiments conducted at the University of Rochester Medical Center were approved by the
410 University of Rochester Committee on Animal Resources.

411 MRI scans

412 Scans were performed on a 9.4 T animal scanner (BioSpec 94/30USR, Bruker BioSpin,
413 Ettlingen, Germany) equipped with a cryogenically cooled quadrature-resonator (CryoProbe,
414 Bruker BioSpin). Head movement during scanning was minimized by restraining the animals
415 on an MR-compatible stereotactic holder with ear bars. During MRI scanning, the animal was
416 anesthetized under 1-1.5% isoflurane in a 1/1 mixture of air/oxygen delivered via nose cone.
417 Cardiac and breathing rate was monitored, and body temperature was maintained at 37 ºC
418 for the duration of the experiment of live imaging (SA Instruments). For brain and CSF volume
419 measurement, a 3D constructive interference in steady-state (3D-CISS) image was calculated
420 as a maximum intensity projection (MIP) from 4 realigned 3D true fast imaging with steady
421 precession (3D-TrueFISP) volumes with 4 orthogonal phase encoding directions (repetition
422 time = 4 ms, echo time = 2 ms, repetitions = 2, flip angle = 40º, spatial resolution 75 µm × 75
423 µm × 75 µm, RF phase advance 0, 180, 90, 270º, total acquisition time = 46 minutes) (32).
424 After the live imaging session, the animal was allowed to inspire 100% nitrogen delivered via
425 a nose cone, which was firmly placed around the mouse's snout, and cardiorespiratory arrest
426 was confirmed (22). The 3D-CISS scanning was repeated at 1, 2, 6, 12, 18, and 24 h after
427 cardiorespiratory arrest. To obtain optimal spatial uniformity, all acquired 3D-TrueFISP
428 volumes were motion-corrected before calculation as MIP, and the image bias field was
429 removed with the N4 bias field correction algorithm of SimpleITK (33, 34). For each brain

430 sample, the total brain volume was automatically segmented by using region growing with
431 ITK-snap (version 3.8.0) (35). In addition, the pixel intensity factorized semi-automatic
432 thresholding was performed to segment the CSF space (including ventricles and subarachnoid
433 spaces) in each hemisphere. The segmentation and volume measurements were performed
434 in Imalytics Preclinical software (ver. 3.0.2.5, Gremse-IT GmbH, Aachen, Germany).

435 Cisterna Magna Infusion

436 Mice were anesthetized by injecting ketamine and xylazine mixture (K/X: 100 mg/kg, 20
437 mg/kg) intraperitoneally (i.p.). Additional anesthesia (K/X: 50 mg/kg, 10 mg/kg) was
438 administered as needed, accompanied by ongoing maintenance and monitoring body
439 temperature at 37 °C. The anesthetized Prox1-eGFP mice were placed in a stereotaxic frame,
440 with the head tilted down in concord position. Then, the skin covering the back of the neck
441 was shaved and opened to visualize the underlying muscles, and dissected to visualize the
442 cisterna magna. A 30G-needle attached to a PE-10 line containing either Evans Blue [0.9kDa,
443 0.5% (w/v) in aCSF] or Bovine Serum Albumin tagged with Alexa 647 [67kDa, 0.5% (w/v) in 2%
444 gelatin in aCSF] was then inserted and secured in place. After detaching the animals from the
445 stereotaxic frame and allowing the recovery of the natural laying down posture, 10 µL, 2
446 µL/min, were infused into the cisterna magna with a syringe pump (Harvard Apparatus) as
447 described before (36). 30 minutes after the start of the infusion, animals were transcardially
448 perfused with 20 mL of PBS to eliminate any blood present in the tissue and brains were
449 quickly extracted. Tracer influx into the brain was imaged ex vivo by macroscopic whole-brain
450 (Leica M205 FA with a Hamamatsu ORCA-Flash4.0 V2 Digital CMOS camera using LAS X Leica
451 software).

452 Whole mount brain and skull immunohistochemistry and imaging

453 Both wildtype C57BL/6JRj and Prox1-EGFP+ mice were anesthetized using ketamine/xylazine
454 (100/20 mg/kg) and the cisterna magna was cannulated for tracer infusion (10µL, 2µL/min,
455 70kDa Texas Red-Dextran. 0.5% (w/v) in aCSF). The tracer was allowed to circulate for 30
456 minutes, and 5 minutes before the sacrifice, 100mL of Wheat Germ Agglutinin conjugated to
457 AlexaFluor-647 (1mg/mL in PBS) was injected retro-orbitally to label the vasculature. Mice
458 were then perfused with 20mL ice cold PBS, then brains were carefully dissected to preserve
459 the dura membrane on the skull surface, and SLYM membrane on the brain surface. Brains,
460 skulls, and livers were immersion fixed in 4% paraformaldehyde in PBS overnight at 4C.
461 For immunohistochemistry, whole brains were cut in half sagittally, and muscle and skin
462 dissected off skulls. Whole mount brains and skulls underwent the same
463 immunohistochemistry treatment. Samples were washed 3 times in PBS and blocked at room
464 temperature for 1hr in blocking solution (5% Normal Donkey Serum, 0.3% Triton, 3% Fab, 0.2%
465 Gelatin in PBS). The samples were then washed 3 times in PBS, then immersed in primary
466 antibody solution overnight on an orbital shaker at 4C (5% Normal Donkey Serum, 0.3% Triton,
467 0.2% Gelatin, 1:200 goat anti-Dpp4 (R&D Biosystems, AF954)). Samples were washed 3 times
468 in PBS and incubated in secondary antibody solution for 2 hours at room temperature on an
469 orbital shaker (5% Normal Donkey Serum, 0.3% Triton, 0.2%Gelatin, 1:500 donkey-ani-goat-
470 Cy2 (705-225-147 Jackson Immunoresearch)). Samples were then washed 3 times in PBS and
471 imaged immediately.
472 Brains and skulls from wildtype mice stained for DDP4 were first imaged on a fluorescent
473 macroscope (LAS-X software; Leica, M205FA). Then brains and skulls were placed in a 2 well
474 chamber with glass coverslip bottom (thickness #1.5H, 80287, Ibidi) and filled with PBS
475 solution. Confocal images were acquired with an Olympus Fluoview microscope (Objective:
476 10x 0.4N.A. Olympus), and Z-stacks were acquired of dorsal and ventral brain and skull

477 surfaces. 2-Photon images were acquired with a resonant scanner B scope (Thorlabs), a 20x
478 Objective (1.0N.A. water dipping, Olympus) and a tunable pulsed laser (Chameleon Ultra II,
479 Coherent). Sequential z-stacks were acquired (ThorImage) at 890nm for second harmonic
480 excitation of collagen fibers, and at 820nm for simultaneous excitation of WGA-647, TxRed-
481 Dextran, and Cy2 antibody. Sequential stacks were aligned using ImageJ software. Prox1-eGFP
482 positive mice were imaged identically, but not stained for DPP4.

483 Immunohistochemistry of paraffin-embedded sections

484 Paraffin-embedded sections from C57BL/6JRj mice were processed according to standard
485 protocols. In brief, endogenous peroxidase activity was quenched and non-specific binding
486 was inhibited by incubation for 30 minutes with 10% goat serum (Biological Industries, Kibbutz
487 Beit-Haemek, Israel) at RT. Sections were incubated overnight at 4 °C with primary antibodies
488 diluted in 10% goat serum and washed with Tris buffered saline (pH 7.4). For subsequent
489 bright-field light microscopy analysis the REALTM EnVisionTM Detection System, consisting of
490 peroxidase/diaminobenzidine+ (DAB+) rabbit/mouse (K5007, Dako, Glostrup, Denmark), was
491 used to detect the primary antibodies. The paraffin sections were counterstained with
492 Mayer`s hematoxylin, dehydrated in graded alcohols, and cover-slipped with Pertex mounting
493 medium (for details on bright-field microscopy, see (38)). Additionally, the entire heads and
494 torsos from perfusion-fixed Prox1-EGFP+ mice were decalcified over three weeks with 10%
495 EDTA in Tris buffer (pH 7) at RT, prior to paraffin embedding and serial sectioning. Sections
496 were processed for immunohistochemistry for EGFP protein detection as described above. A
497 list of the primary antibodies used can be found in Table 1.

498

499

Antigen	Immunogen	Manufacturer (CAT#)	Host & isotype	Dilution	Reference RRID#
Aquaporin-1 (AQP-1)	19-aa peptide of Rat AQP1 Target epitope is in C-terminus, intracellular	Alpha Diagnostics (AQP11-A)	Rabbit IgG	1:800	AB_1609286
Aquaporin-4 (AQP-4)	Synthetic peptide corresponding to a sequence at the C-terminus of human Aquaporin 4	Aviva Systems Technology (OABB01958)	Rabbit IgG	1:3000	
Cellular retinoic acid-binding protein 2 (CRABP2)	CRABP2 fusion protein Ag0309	Proteintech (10225-1-AP)	Rabbit IgG	1:200	AB_2085455
Claudin-11 (CLDN-11)	Synthetic peptide corresponding to human oligodendrocyte specific protein (C terminal)	Abcam (ab53041)	Rabbit IgG	1:400	AB_2276205
Dipeptidyl peptidase IV (DPP4)	Mouse myeloma cell line NS0-derived recombinant mouse DPPIV/CD26 Ser29-His760 Accession # P28843	R&D Systems (AF594)	Goat IgG	1:200	AB_355739
E-Cadherin (E-Cad)	Recombinant full length protein	Abcam (ab231303)	Mouse IgG1	1:100	AB_2923285
Fibroblast Antibody (ER-TR7)	Isolated C3H thymic stromal cells	Novus (NB100-64932)	Rat IgG2a	1:300	AB_963381
Green fluorescent protein (GFP)	GFP isolated directly from Aequorea victoria	Thermo Fischer Scientific (A-6455)	Rabbit IgG	1:1000-1:2000	AB_221570
Lymphatic vessel endothelial hyaluronan receptor 1 (LYVE 1)	Recombinant fragment His-Tag corresponding to Mouse LYVE1 aa 1-250 (C terminal)	Abcam (ab14917)	Rabbit IgG	1:100	AB_301509

Plectin [E398P]	Recombinant fragment	Abcam (ab32528)	Rabbit IgG	1:250	AB_777339
Podoplanin (PDPN)	Murine thymic stromal cell lines	Thermo Fischer Scientific (14-5381-85)	Syrian Hamster IgG	1:200	AB_1210507
Prospero homeobox 1 (Prox1)	Recombinant fragment	Abcam (ab199359)	Rabbit IgG	1:200	AB_2868427
Retinaldehyde dehydrogenase 2 (RALDH2)	Retinal dehydrogenase 2 recombinant protein epitope signature tag (PrEST)	Sigma Life Science (HPA010022)	Rabbit IgG	1:500	AB_1844723

List of abbreviations

ABC layer: Arachnoid Barrier Cell Layer
CiA: cisterna ambiens
CiC: Cisterna caroticus
CiP: cisterna pontis
CLDN-11: Claudin 11
CRABP2: Cellular retinoic acid-binding protein 2
DPP4: Dipeptidyl peptidase IV
LYVE1: Lymphatic vessel endothelial hyaluronan receptor 1
PBS: Phosphate Buffered Saline
PDPN: Podoplanin
RALDH2: Retinaldehyde dehydrogenase 2
SAS: Subarachnoid Space
SLYM: Sub-arachnoid Lymphatic-like Membrane
VEGFRC: Vascular endothelial growth factor

Declarations

Ethics approval and consent to participate

All experiments carried out at the University of Copenhagen were approved by the Animal Experiments Council under the Danish Ministry of Environment and Food (license number: 2015-15-0201-00535) and the procedures were performed in accordance with the European directive 2010/63/EU, with an effort was undertaken to reduce the utilization of animals. This study does not involve human participants, human data or human tissue, thus consent to participate is not applicable.

Consent for publication

Not applicable

Availability of data and materials

The datasets used and/or analyzed during the current study are available from the corresponding author on reasonable request.

Competing interests

The authors declare that they have no competing interests

Funding

Funding was provided by Lundbeck Foundation grant R386-2021-165 (M.N.), Novo Nordisk Foundation grant NNF20OC0066419 (M.N.), the Vera & Carl Johan Michaelsen's Legat Foundation (K.M.), National Institutes of Health grant R01AT011439 (M.N.), National Institutes of Health grant U19NS128613 (M.N.), US Army Research Office grant MURI W911NF1910280 (M.N.), Human Frontier Science Program grant RGP0036 (M.N.), the Dr. Miriam and Sheldon G. Adelson Medical Research Foundation (M.N.), and Simons Foundation grant 811237 (M.N.). The views and conclusions contained in this article are solely those of the authors and should not be interpreted as representing the official policies, either expressed or implied, of the National Institutes of Health, the Army Research Office, or the US Government. The US Government is authorized to reproduce and distribute reprints for Government purposes notwithstanding any copyright notation herein. The funding agencies have taken no part on the design of the study, data collection, analysis, interpretation, or in writing of the manuscript.

Authors' contributions

KM: Conceptualization, Funding acquisition, Investigation, Methodology, Project administration, Resources, Supervision, Validation, Visualization, Writing - original draft, and Writing - review & editing.

VP: Investigation, Methodology, Project administration, Validation, Visualization, Writing - original draft, and Writing - review & editing.

MG, AL, DG: Investigation, Methodology, Visualization, and Writing - review & editing.

SB: Investigation, Writing - review & editing.

MN: Conceptualization, Formal analysis, Funding acquisition, Methodology, Project administration, Resources, Supervision, Validation, Visualization, Writing - original draft, and Writing - review & editing.

YM: MRI image acquisition and analysis

Acknowledgments: We acknowledge P. S. Froh (Department of Cellular and Molecular Medicine, Faculty of Health and Medical Sciences, University of Copenhagen, Denmark) for excellent technical assistance with the histology and immunohistochemistry of the decalcified samples. We also thank D. Xue for expert graphical support.

References

1. Rasmussen MK, Mestre H, Nedergaard M. Fluid transport in the brain. Physiological reviews. 2022;102(2):1025-151.
2. Louveau A, Smirnov I, Keyes TJ, Eccles JD, Rouhani SJ, Peske JD, et al. Structural and functional features of central nervous system lymphatic vessels. Nature. 2015;523(7560):337-41.
3. Harrison IF, Ismail O, Machhada A, Colgan N, Ohene Y, Nahavandi P, et al. Impaired glymphatic function and clearance of tau in an Alzheimer's disease model. Brain : a journal of neurology. 2020;143(8):2576-93.
4. McKnight CD, Trujillo P, Lopez AM, Petersen K, Considine C, Lin Y-C, et al. Diffusion along perivascular spaces reveals evidence supportive of glymphatic function impairment in Parkinson disease. Parkinsonism & related disorders. 2021;89:98-104.
5. Jiang D, Liu L, Kong Y, Chen Z, Rosa-Neto P, Chen K, et al. Regional Glymphatic Abnormality in Behavioral Variant Frontotemporal Dementia. Annals of neurology.n/a(n/a).
6. Lynch M, Pham W, Sinclair B, O'Brien TJ, Law M, Vivash L. Perivascular spaces as a potential biomarker of Alzheimer's disease. Frontiers in neuroscience. 2022;16.
7. Liu H, Chen L, Zhang C, Liu C, Li Y, Cheng L, et al. Interrogation of dynamic glucose-enhanced MRI and fluorescence-based imaging reveals a perturbed glymphatic network in Huntington's disease. bioRxiv. 2023:2023.04.03.535397.
8. Nedergaard M, Goldman SA. Glymphatic failure as a final common pathway to dementia. Science. 2020;370(6512):50-6.
9. Benias PC, Wells RG, Sackey-Aboagye B, Klavan H, Reidy J, Buonocore D, et al. Structure and Distribution of an Unrecognized Interstitium in Human Tissues. Scientific reports. 2018;8(1):4947.
10. Mestre H, Tithof J, Du T, Song W, Peng W, Sweeney AM, et al. Flow of cerebrospinal fluid is driven by arterial pulsations and is reduced in hypertension. Nature communications. 2018;9(1):4878.
11. Mestre H, Mori Y, Nedergaard M. The Brain's Glymphatic System: Current Controversies. Trends in neurosciences. 2020;43(7):458-66.
12. Møllgård K, Beinlich FRM, Kusk P, Miyakoshi LM, Delle C, Plá V, et al. A mesothelium divides the subarachnoid space into functional compartments. Science. 2023;379(6627):84-8.
13. Ducoli L, Detmar M. Beyond PROX1: transcriptional, epigenetic, and noncoding RNA regulation of lymphatic identity and function. Developmental Cell. 2021;56(4):406-26.
14. Choi I, Chung HK, Ramu S, Lee HN, Kim KE, Lee S, et al. Visualization of lymphatic vessels by Prox1-promoter directed GFP reporter in a bacterial artificial chromosome-based transgenic mouse. Blood. 2011;117(1):362-5.
15. Mathiesen BK, Miyakoshi LM, Cederroth CR, Tserga E, Versteegh C, Bork PAR, et al. Delivery of gene therapy through a cerebrospinal fluid conduit to rescue hearing in adult mice. Science translational medicine. 2023;15(702):eabq3916.
16. Johanson CE. J Choroid Plexus–Cerebrospinal Fluid Circulatory Dynamics: Impact on Brain Growth, Metabolism, and Repair. P.M. C, editor. Totowa, NJ: Humana Press; 2008.
17. Eide PK, Vinje V, Pripp AH, Mardal KA, Ringstad G. Sleep deprivation impairs molecular clearance from the human brain. Brain : a journal of neurology. 2021;144(3):863-74.

18. Mapunda JA, Pareja J, Vladymyrov M, Bouillet E, Helie P, Pleskac P, et al. VE-cadherin in arachnoid and pia mater cells serves as a suitable landmark for in vivo imaging of CNS immune surveillance and inflammation. Nature communications. 2023;14(1):5837.
19. Pietila R, Del Gaudio F, He L, Vazquez-Liebanas E, Vanlandewijck M, Muhl L, et al. Molecular anatomy of adult mouse leptomeninges. Neuron. 2023.
20. Nabeshima S, Reese TS, Landis DM, Brightman MW. Junctions in the meninges and marginal glia. The Journal of comparative neurology. 1975;164(2):127-69.
21. Orlin JR, Osen KK, Hovig T. Subdural compartment in pig: a morphologic study with blood and horseradish peroxidase infused subdurally. The Anatomical record. 1991;230(1):22-37.
22. Du T, Mestre H, Kress BT, Liu G, Sweeney AM, Samson AJ, et al. Cerebrospinal fluid is a significant fluid source for anoxic cerebral oedema. Brain : a journal of neurology. 2022;145(2):787-97.
23. Louveau A, Filiano AJ, Kipnis J. Meningeal whole mount preparation and characterization of neural cells by flow cytometry. Curr Protoc Immunol. 2018;121(1):e50.
24. Brøchner CB, Holst CB, Møllgård K. Outer brain barriers in rat and human development. Frontiers in neuroscience. 2015;9.
25. Liliequist B. The anatomy of the subarachnoid cisterns. Acta radiol. 1956;46(1-2):61-71.
26. Volovici V, Varvari I, Dirven CMF, Dammers R. The membrane of Liliequist-a safe haven in the middle of the brain. A narrative review. Acta Neurochir (Wien). 2020;162(9):2235-44.
27. Yasargil MG, Kasdaglis K, Jain KK, Weber HP. Anatomical observations of the subarachnoid cisterns of the brain during surgery. Journal of neurosurgery. 1976;44(3):298-302.
28. Lopes CA, Mair WG. Ultrastructure of the arachnoid membrane in man. Acta Neuropathol. 1974;28(2):167-73.
29. Krisch B, Leonhardt H, Oksche A. The meningeal compartments of the median eminence and the cortex. A comparative analysis in the rat. Cell Tissue Res. 1983;228(3):597-640.
30. Krisch B, Leonhardt H, Oksche A. Compartments and perivascular arrangement of the meninges covering the cerebral cortex of the rat. Cell Tissue Res. 1984;238(3):459-74.
31. Vandenabeele F, Creemers J, Lambrichts I. Ultrastructure of the human spinal arachnoid mater and dura mater. J Anat. 1996;189 (Pt 2)(Pt 2):417-30.
32. Gomolka RS, Hablitz LM, Mestre H, Giannetto M, Du T, Hauglund NL, et al. Loss of aquaporin-4 results in glymphatic system dysfunction via brain-wide interstitial fluid stagnation. eLife. 2023;12.
33. Tustison NJ, Avants BB, Cook PA, Zheng Y, Egan A, Yushkevich PA, et al. N4ITK: improved N3 bias correction. IEEE Trans Med Imaging. 2010;29(6):1310-20.
34. Yaniv Z, Lowekamp BC, Johnson HJ, Beare R. SimpleITK Image-Analysis Notebooks: a Collaborative Environment for Education and Reproducible Research. J Digit Imaging. 2018;31(3):290-303.
35. Yushkevich PA, Piven J, Hazlett HC, Smith RG, Ho S, Gee JC, et al. User-guided 3D active contour segmentation of anatomical structures: significantly improved efficiency and reliability. NeuroImage. 2006;31(3):1116-28.

36. Iliff JJ, Wang M, Liao Y, Plogg BA, Peng W, Gundersen GA, et al. A paravascular pathway facilitates CSF flow through the brain parenchyma and the clearance of interstitial solutes, including amyloid β. Sci Transl Med. 2012;4(147):147ra11.
37. Mestre H, Du T, Sweeney AM, Liu G, Samson AJ, Peng W, et al. Cerebrospinal fluid influx drives acute ischemic tissue swelling. Science. 2020;367(6483).
38. Møllgård K, Dziegielewska KM, Holst CB, Habgood MD, Saunders NR. Brain barriers and functional interfaces with sequential appearance of ABC efflux transporters during human development. Scientific reports. 2017;7(1):11603.

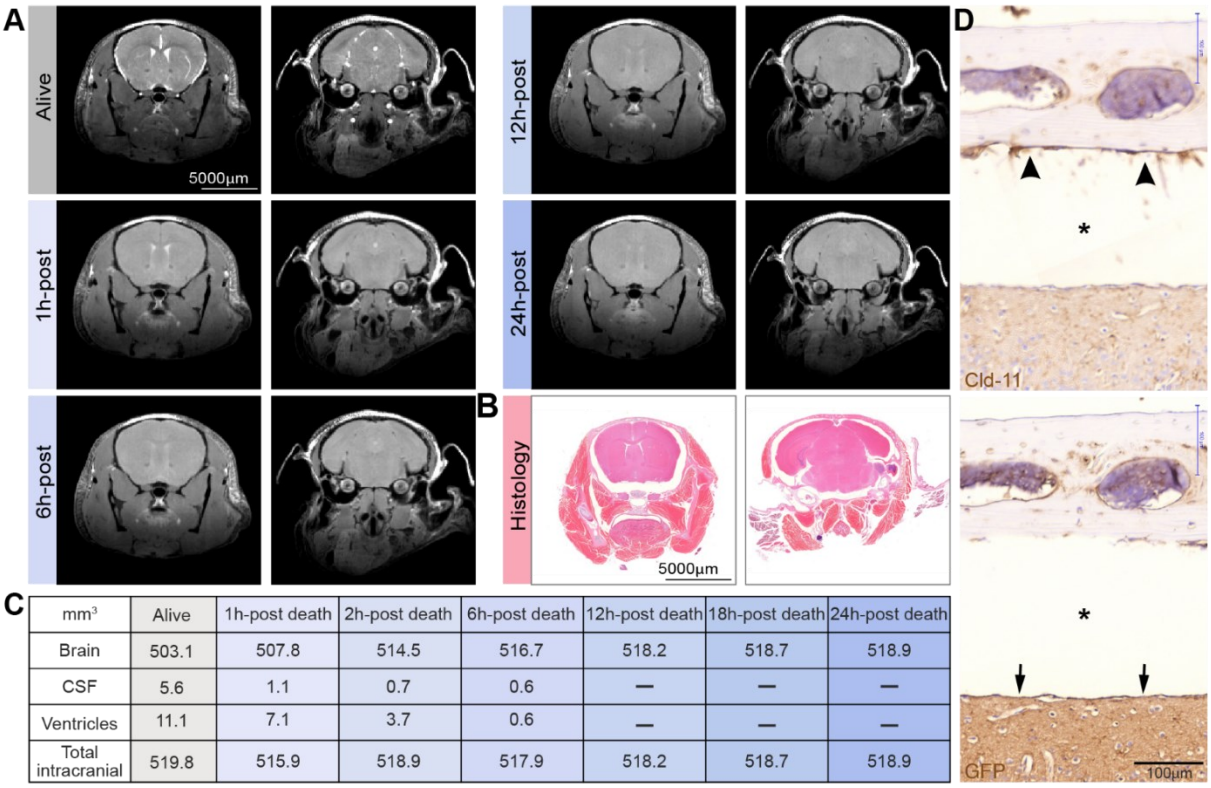

C

mm³	Alive	1h-post death	2h-post death	6h-post death	12h-post death	18h-post death	24h-post death
Brain	503.1	507.8	514.5	516.7	518.2	518.7	518.9
CSF	5.6	1.1	0.7	0.6	—	—	—
Ventricles	11.1	7.1	3.7	0.6	—	—	—
Total intracranial	519.8	515.9	518.9	517.9	518.2	518.7	518.9

Fig. 1. Preparation of histological sections is linked to a marked shrinkage of the brain's fluid-filled spaces (A) Magnetic resonance imaging (MRI) of a young C57BL/6JRj mouse shows that CSF in the subarachnoid space and the ventricles in a live isoflurane anesthetized mouse gradually disappear after death, indicative of brain swelling. After the live imaging session, the anesthetized mouse was killed by 100% nitrogen inhalation via a nose cone on an MR-compatible stereotactic holder, and scanning was repeated at 1, 2, 6, 12, 18, and 24 h after cardiorespiratory arrest. (**B**) Histological section of the head of a young C57BL/6JRj mouse after decalcification and preparation of parafin. **(C)** Quantification of the volume of the brain, the subarachnoid space, the ventricles and total intracranial volume based on the images displayed in panel A. **(D)** Immunohistochemical analysis of arachnoid barrier cell layer (top, arrowheads) stained for Cld-11 and SLYM stained for GFP (lower, arrows) in two consecutive sections prepared from a Prox1-eGFP mouse. Note the considerable shrinkage of the brain (asterisk) in the sections.

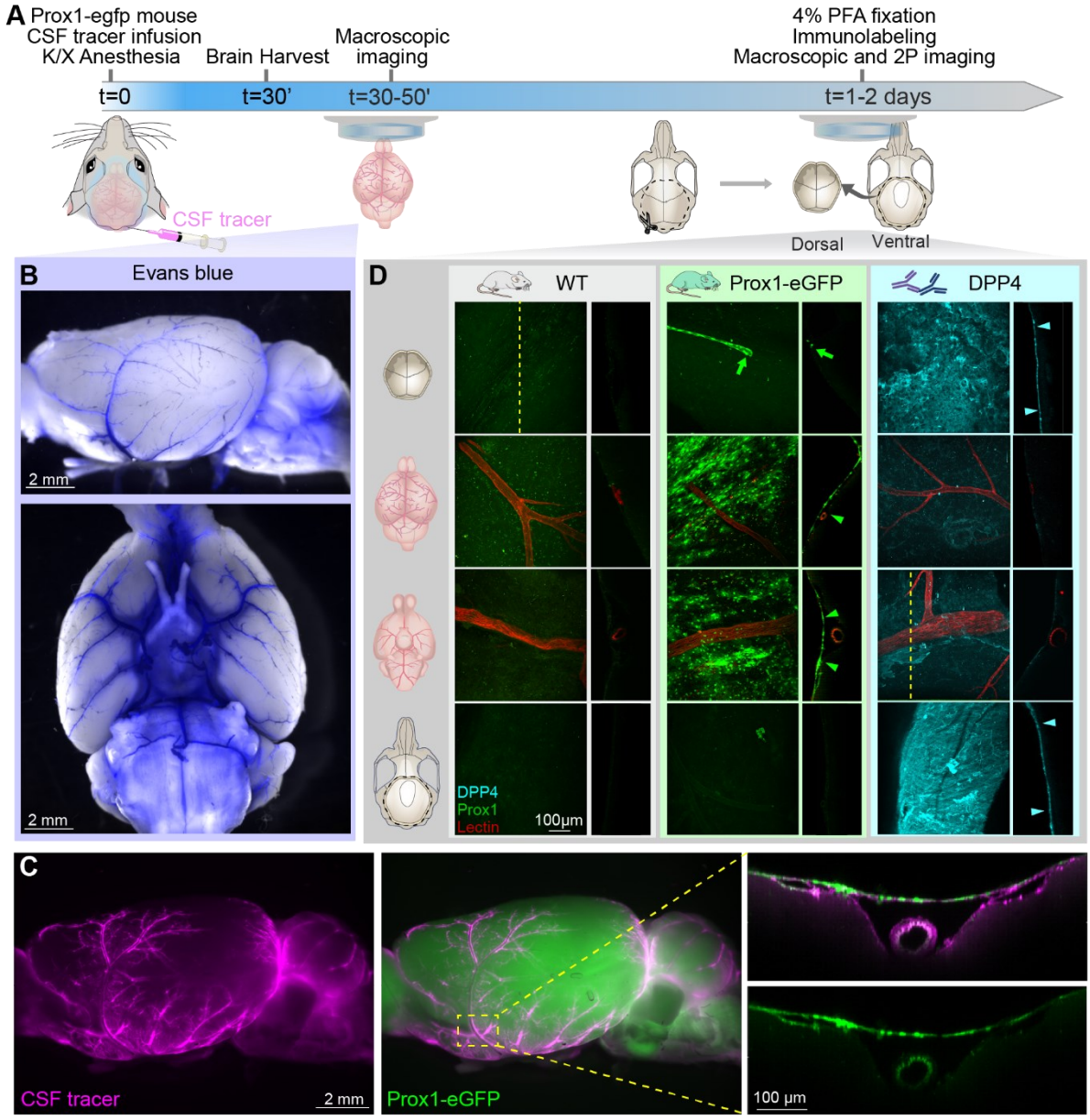

Fig. 2: SLYM defines the subarachnoid cisternal system and the pial perivascular space. **(A)** Schematic of the experimental approach. CSF tracers, either Evans Blue (0.9 kDa, 0.5% in aCSF w/v) or BSA-647 (67 kDa, 0.5% w/v) were delivered (10 µL, 2 µL/min) through a cisterna magna cannula in K/X-anesthetized Prox1-eGFP mice. After 30 minutes of tracer circulation, the PROX1-eGFP mice were perfused with PBS to remove blood signal interference. The brains were imaged immediately after harvesting using a fluorescent macroscope. **(B)** Macroscopic fluorescent images of the whole brain showing the cisterns and pial perivascular spaces filled with a small size tracer, Evans blue (blue). **(C)** Representative images of a brain from an animal injected with a larger tracer, BSA-647 (magenta). The green signal corresponds to Prox1-eGFP expression. Close-up images over a major cerebral artery (middle cerebral artery) illustrate the accumulation of the fluorescent tracer below the Prox1-eGFP+ cells. **(D)** Skull and brain from both Prox1-eGFP and wildtype mice taken before and after DPP4 staining. Confocal and two-photon XY projections from whole-mount dorsal skull (first row), dorsal brain (second row), ventral brain (third row), and ventral skull (bottom row). Orthogonal projections were obtained as indicated by the dashed line in the first panel, except for the ventral brain after DPP4 staining where the projection was obtained from an area

including a DPP4 positive section close to the vessel. A meningeal lymphatic vessel positive for Prox1-eGFP is observed in the dorsal skull of the Prox1-eGFP mouse (green arrow). The analysis showed that SLYM in the Prox1-eGFP reporter mice (green arrowheads) adheres to the brain surface, whereas the ABC layer, immunolabeled for DPP4 (cyan arrowheads), adheres to dura on the skull.

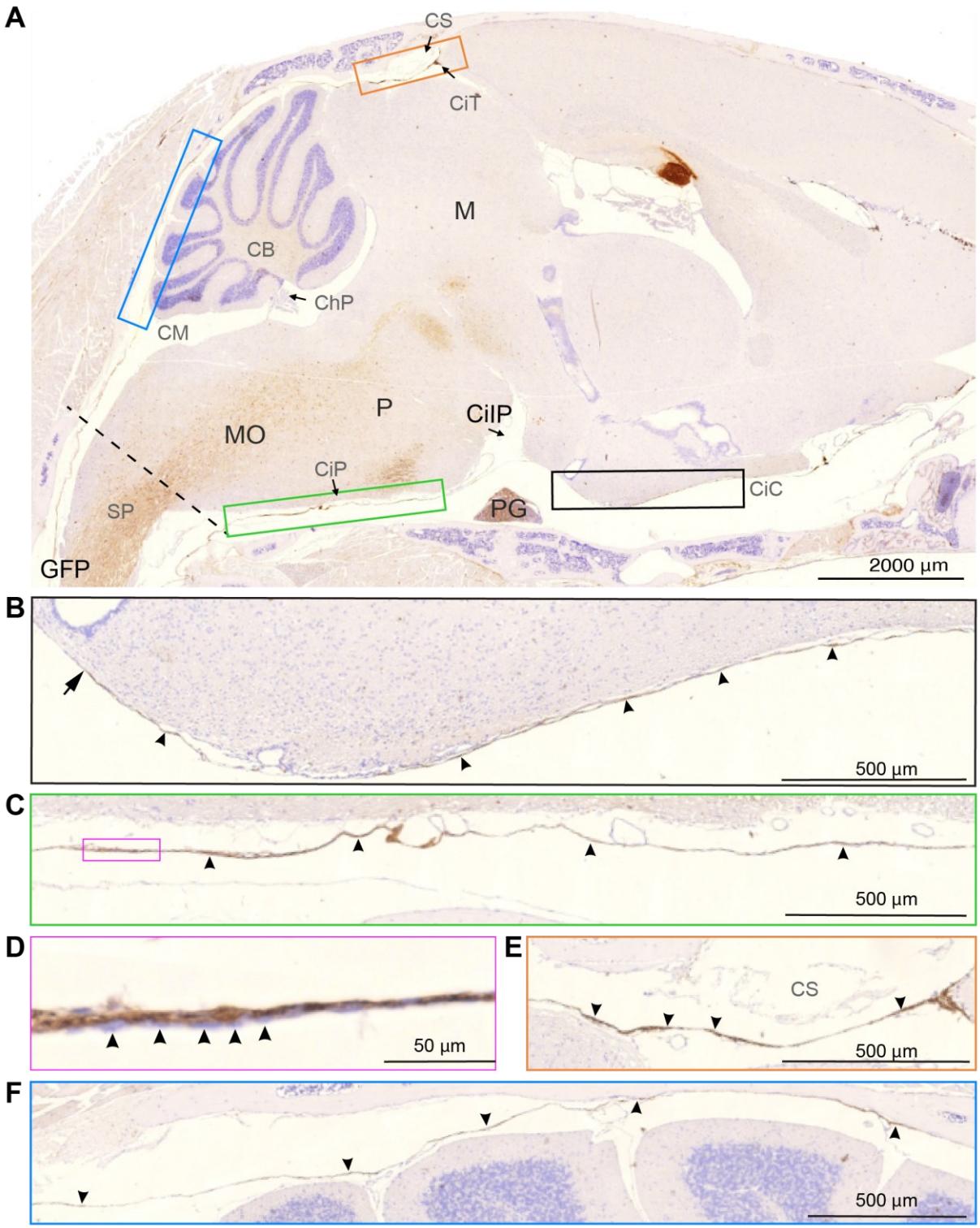

Fig. 3: SLYM encases the brain parenchyma here shown in a sagittal section extending caudally from the upper spinal cord to the olfactory bulb region rostral. (A) GFP immunosignal in Prox1-eGFP mouse tissue forms a lamina covering the entire brain, delimiting the cisternal spaces. Colored insets are used to show high magnification images of different anatomical regions. The dashed line indicates the plane through foramen magnum separating the spinal cord (SP) from medulla oblongata (MO). **(B) Black insert** shows the rostral extension of the basal cistern (arrowheads). Note that the histochemical reactivity is attenuated corresponding to the median eminence (arrow). Cisterna interpeduncularis (CiIP) has been

698 already analyzed in a previous publication (Møllgård, et al., 2023 (12), suppl fig.3). **(C) The**
699 **green insert** depicts the cisterna pontis (CiP), lining the basal CSF space. **(D)** In a higher
700 magnification (**magenta insert**) SLYM, with individual GFP positive cells (arrowheads),
701 seems to be partly covered by an inner cell layer to the left. **(E) Orange insert** shows the region
702 of confluence of sinuses (CS) where the GFP signal is clearly visible **(arrowheads),** delimiting
703 the cisterna tegmentalis (CiT). **(F) Blue insert** shows the superior cerebellar cistern (cisterna
704 vermis), delimiting two CSF spaces adjacent to the cerebellum. The one-layered delicate
705 SLYM membrane deviates between attachment to the skull and the cerebellar pial surface.

706 CB: cerebellum, ChP: choroid plexus, CiC: carotidand chiasmatic cistern, CiIP: cisterna
707 interpeduncularis. CiP: cisterna pontis, CiI: cisterna tegmentalis, CM: cisterna magna, CS:
708 confluence sinuum, M: mesencephalon, MO: medulla oblongata, P: pons, PG: pituitary gland,
709 SP: spinal cord. Magnification is indicated by labelled bars on the individual figures.

710

a

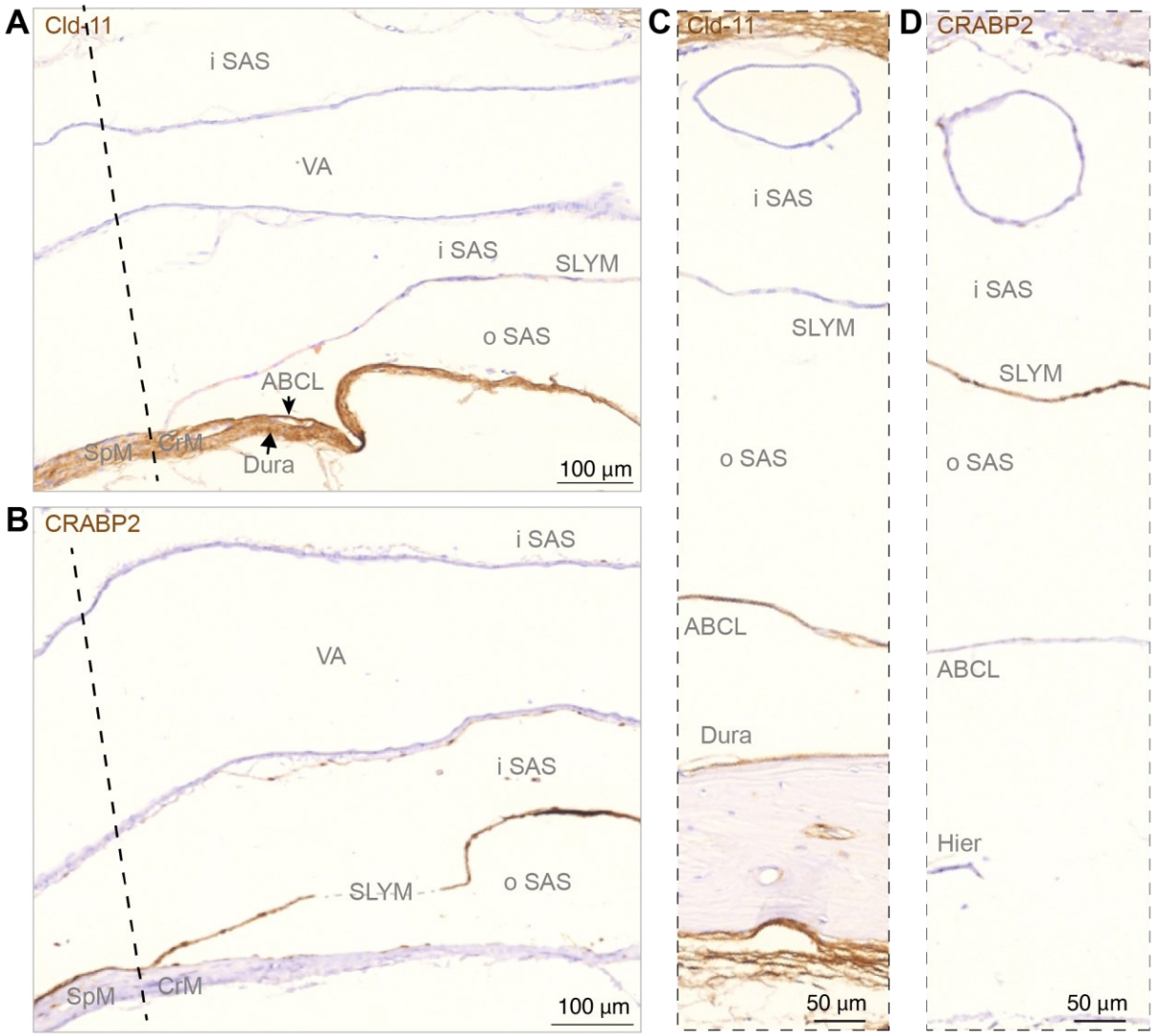

Fig. 4: Sagittal sections show SLYM is not fused with the arachnoid barrier layer along basal cisterns. **(A, B)** Immunohistochemical analysis of arachnoid barrier cell layer (ABCL) stained for Cld-11 and SLYM stained for CRABP2 at the transition from spinal meninges (SpM) to cranial meninges (CeM) indicated by dashed line, corresponding to the plane of foramen magnum. SLYM and ABCL are fused corresponding to the rostral-most spinal meninges, but the deviation of the two layers is characteristic of the beginning of cranial meninges creating an inner subarachnoid space (iSAS) containing the vertebral artery (VA) and an outer subarachnoid space, between SLYM and the arachnoid barrier layer. In **(C, D)** corresponding to cisterna pontis the arachnoid barrier cell layer (ABCL), positively reacting for Cld-11, covers dura but renders SLYM negative. SLYM shows positive immunoreactivity for CRABP2 whereas the ABCL is not stained. Due to the heat-induced epitope retrieval (Hier) a fraction of bone with dura disappeared from this section.

Dashed line indicates a nearly frontal plane through foramen magnum separating the spinal cord from medulla oblongata and thus the cranial meninges (CrM) from spinal meninges (SpM).

ABCL: arachnoid barrier cell layer, CrM: cranial meninges, Hiar: heat-induced antigen retrieval, iSAS: inner subarachnoid space, oSAS: outer subarachnoid space, SpM: spinal

730 meninges, VA: vertebral artery. Magnification is indicated by labelled bars on the individual
731 figures.

732

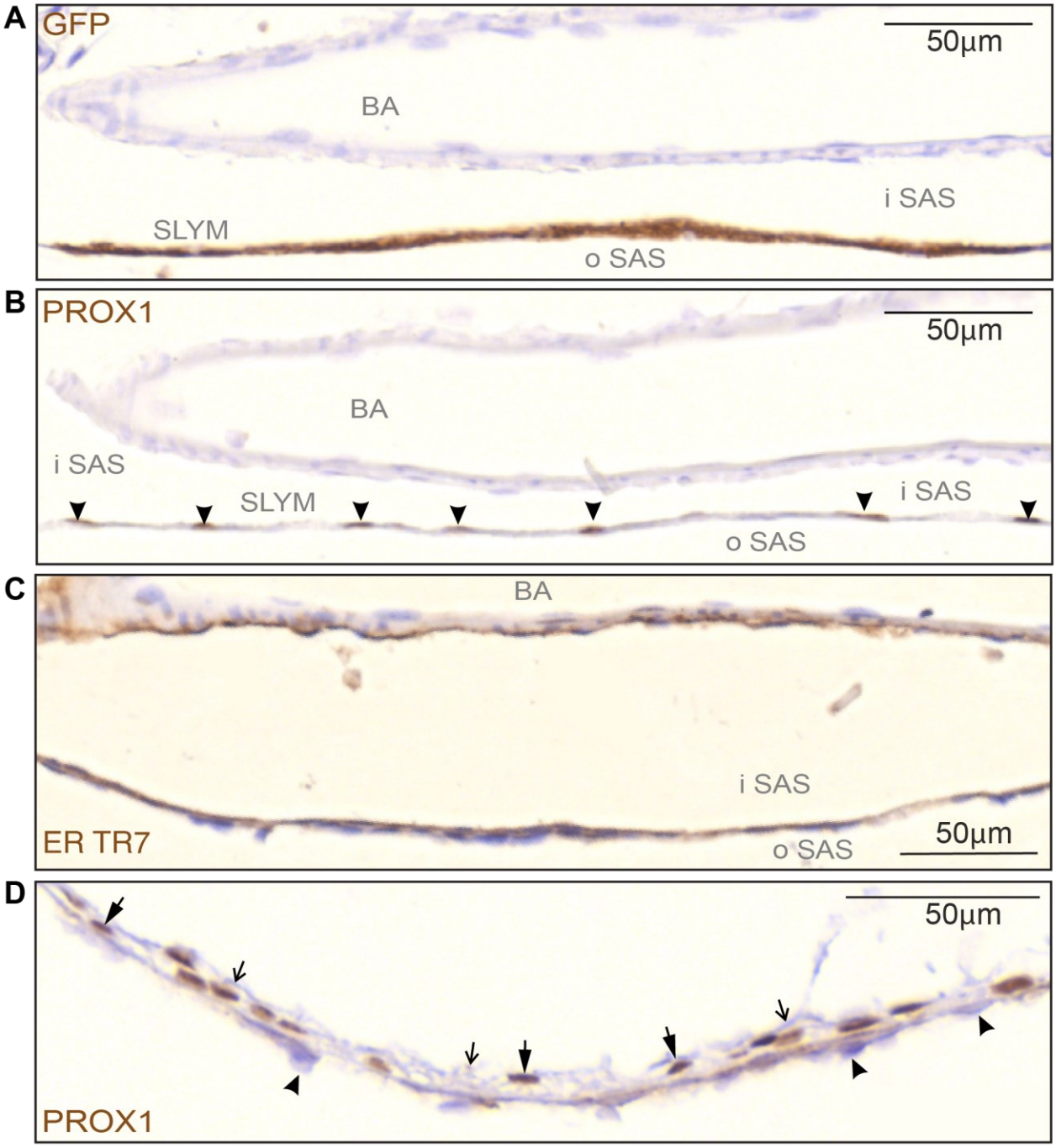

Fig. 5: SLYM is characterized by a specific subset of immunological markers. (A-C) High magnification images of the basilar artery on the ventral part of the brain show the division of the subarachnoid space (SAS) into an outer and inner compartment by the SLYM meningeal layer (GFP+ labelled). **(B)** Prox1 immunolabeling of serial sections of the same tissue allowed individual identification of SLYM cells, due to their immunoreactive nuclei (arrowheads). **(C)** ER-TR7 immunoreactivity is found on the inner surface of SLYM, showing the presence of Collagen type VI on this meningeal layer. Also note the staining of adventitia of the basilar artery (BA). **(D)** The Prox1-stained nuclei (thick arrows) in the wall of cisterna ambiens are in direct contact with arachnoid barrier cells towards the exterior (arrowheads) and with an unstained layer of arachnoid reticular cells facing the inner subarachnoid space (thin, open arrows).

745 BA: basilar artery, iSAS: inner subarachnoid space, oSAS: outer subarachnoid space.
746 Magnification is indicated by labelled bars on the individual figures.

747

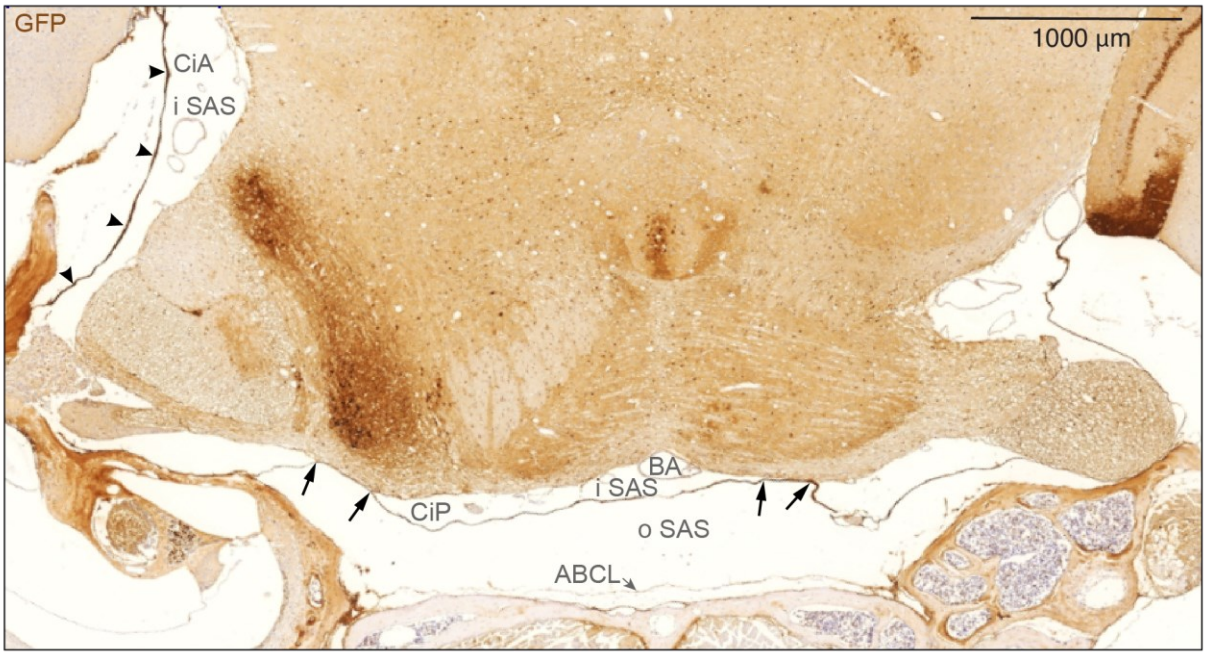

Fig. 6: SLYM encases brain parenchyma evident in a coronal section through mid-pontine region. Immunohistochemical analysis of GFP signal of a coronal section of Prox1-eGFP tissue allowed additional characterization of the meningeal layers covering the parenchyma. SLYM (GFP+) layer divides the subarachnoid space into two well-defined compartments, an outer subarachnoid space (oSAS) facing the arachnoid barrier cell layer (ABCL) and an inner subarachnoid space (iSAS), enclosing blood vessels, here the basilar artery (BA). SLYM seems to fuse with pia covering a fraction of the basolateral part of pons on both sides (arrows) thus creating a sub-compartmentalization of the inner SAS. The strongly stained cisterna ambiens (CiA) is indicated by arrowheads.

ABCL: arachnoid barrier cell layer, BA: basilar artery, CiA: cisterna ambiens, CiP: cisterna pontis, iSAS: inner subarachnoid space, oSAS: outer subarachnoid space. Magnification is indicated by labelled bar.

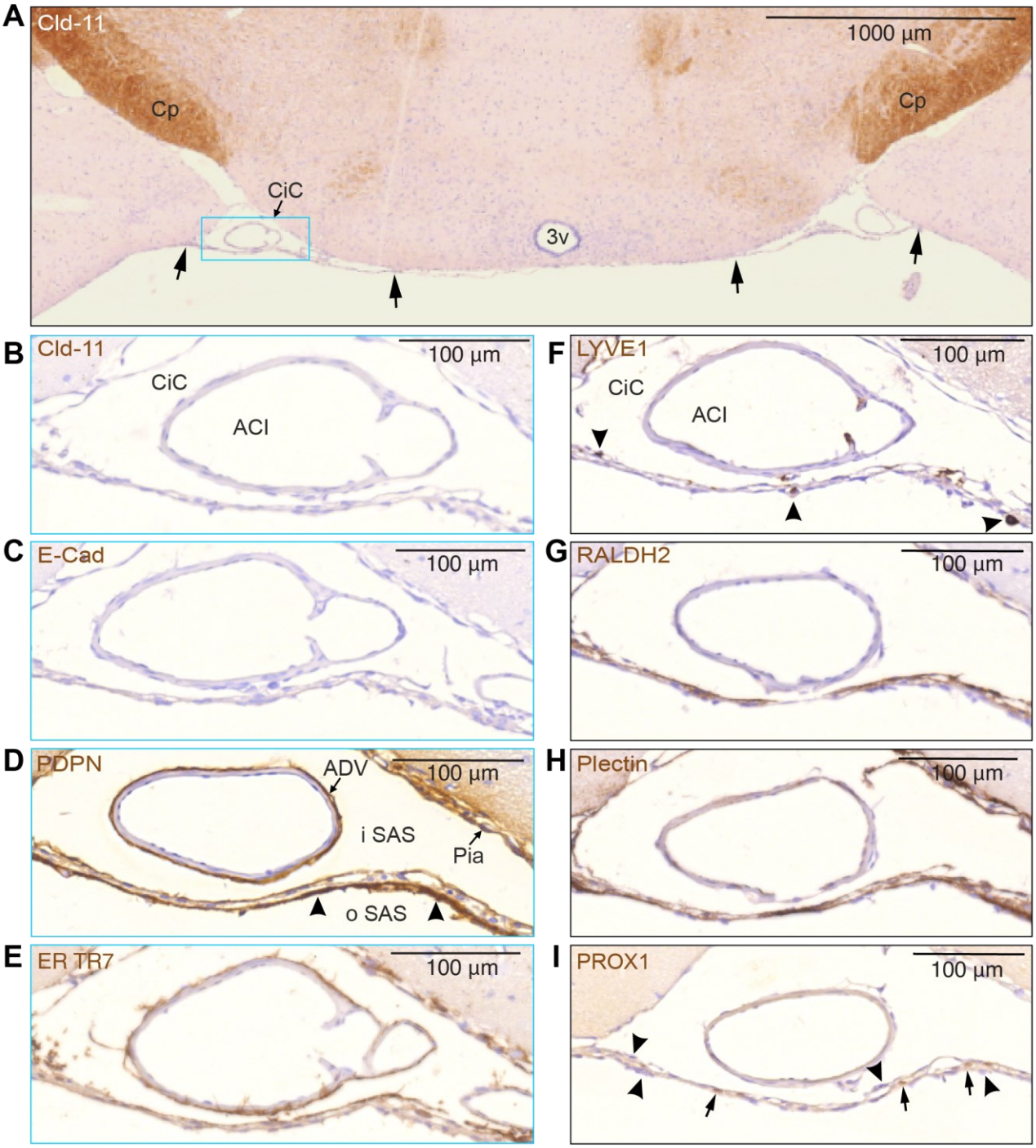

Fig. 7: SLYM and the ABC layer can be differentiated by their distinctive immunomarker expression (A) The unstained SLYM in this claudin-11 stained section located at a middle coronal position of the circle of Willis, at the suprachiasmatic level, indicated by arrows**,** seems to fuse with the pia along both medial and lateral borders of the cisterna caroticus (CiC) - blue rectangle - which is shown in higher magnification in **(B-I)**. Note the positive Cld-11 reactivity in the oligodendrocytes of the cerebral peduncle (Cp) in contrast to the negative appearance of SLYM in **(B). (C)** E-cadherin staining also provided a negative response in SLYM, pia and adventitia of the internal carotid artery (ACI). **(D-I)** show SLYM covered by an inner and outer layer of different types of arachnoid leptomeningeal fibroblasts. The PDPN-stained section **(D)** demonstrates a strongly reactive layer (arrowheads) facing the outer SAS (oSAS), a weaklier stained SLYM in the middle and yet another thin leptomeningeal layer facing the inner SAS

774 (iSAS) with a positively reacting pia. The adventitia (ADV) surrounding the internal carotid
775 artery (ACI in B) is also positively stained. **(E)** ER-TR7 immunoreactivity demonstrates
776 collagen type VI in particular on the inside of SLYM but is also associated with adventitia of
777 ACI and pia. **(F)** As expected by its "lymphatic-like" nature, SLYM acts as an immunological
778 niche. LYVE1 antibody highlights perivascular macrophages (arrowheads) located either on
779 the inner, middle or outer part of SLYM. **(G)** Retinaldehyde dehydrogenase (RALDH2) is
780 particularly strongly stained along the inner SLYM layer. **(H)** Plectin, a possible key
781 cytoskeleton interlinking molecule, is also present in SLYM meningeal lamina, in particular
782 facing the outer subarachnoid space, but also staining the pia. **(I)** PROX1-stains nuclei (arrows)
783 identify SLYM as the middle layer in this triple-layered structure where nuclei in inner and
784 outer layers are PROX1-negative (arrowheads).

785 3v: third ventricle, ACI: internal carotid artery, ADV: adventitia, CiC: cisterna caroticus, Cp:
786 cerebral peduncle. Magnification is indicated by labelled bars on the individual figures.

787

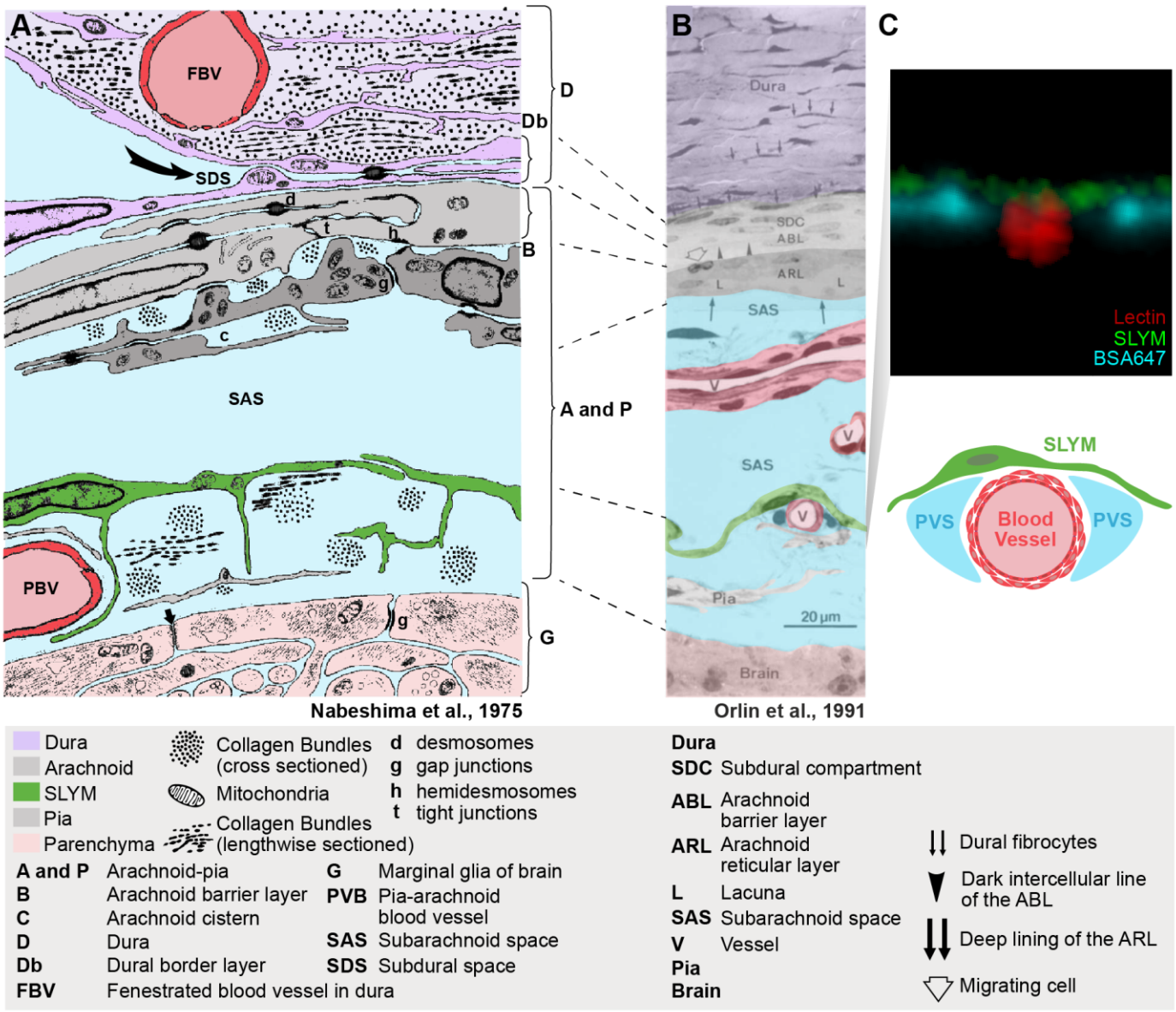

Fig. 8: SLYM is illustrated as a distinctive meningeal layer in the classical literature. (A) Reproduced sketch from Nabeshima et al., 1975 (20). The sketch is based on examination of the meningeal region in studies of multiple mammals (mice, rats, chinchillas, rabbits, cats and Macaque monkeys) by electron microscopy and freeze-fracturing. Meningeal layers have been color-coded for clarity, without changing the original sketch. SLYM layer is already indicated as an intermedial layer between the arachnoid (ABC and ARLlayers) and pia, resting on top of a pial vessel (PBV). **(B)** Light microscopy of a thin section stained with toluidine of meninges in the Norwegian landrace pig image from Orlin et al., 1991 (21). Orlin et al., compared this section to the sketch in the Nabeshima publication and the original labels and lines have not been changed. **(C)** Confocal cross-section of a pial vessel from this study (Fig. S2E) is included to compare the structural details with our observations. The sketch below illustrates that SLYM forms the roof of the pial perivascular spaces.

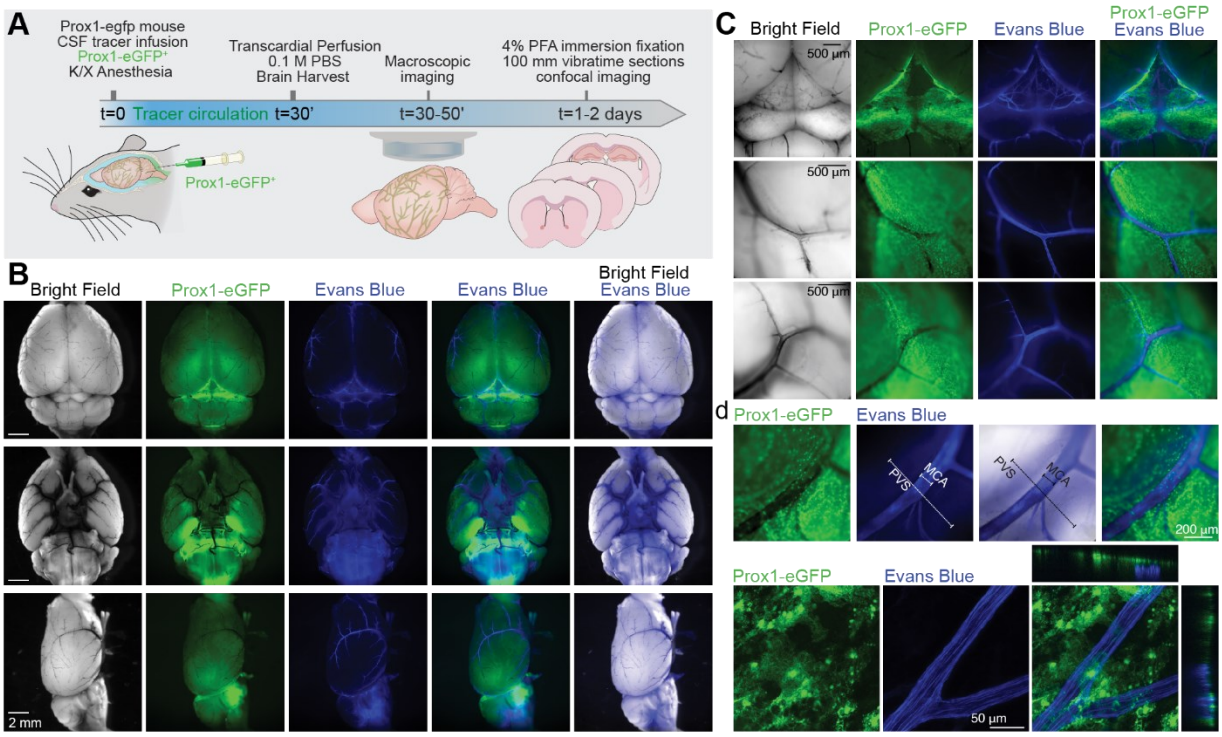

Supplementary Fig. 1: SLYM layer defines the perivascular space. (A) Scheme of the experimental approach. Tracer [Evans Blue, 0.9 kDa, 0.5% in aCSF (w/v), 10 µL, 2 µL/min] was delivered by cisterna magna cannulation to CSF space of K/X-anesthetized Prox1-eGFP mice. After 30 minutes circulation of the tracer, mice were perfused with PBS to eliminate blood vessel signal and brains were extracted and acutely imaged under a fluorescent microscope. **(B)** Macroscope bright field and fluorescent images of the whole brain. Bright field images (grey) show the basal cisterns filled with Evans Blue. Green signal corresponds to Prox1-eGFP expression and Evans Blue fluorescence is additionally shown in blue. **(C)** Close-up images over the pineal gland (dorsal) and MCA (ventral) illustrate the accumulation of Evans Blue in the arterial space, covered by Prox1-eGFP+ cells. **(D)** To evaluate the spatial location of Prox1-eGFP cells regarding MCA, high magnification images were combined with confocal images, where orthogonal views showed the location of Evans Blue signal on the parenchymal side below the SLYM layer.

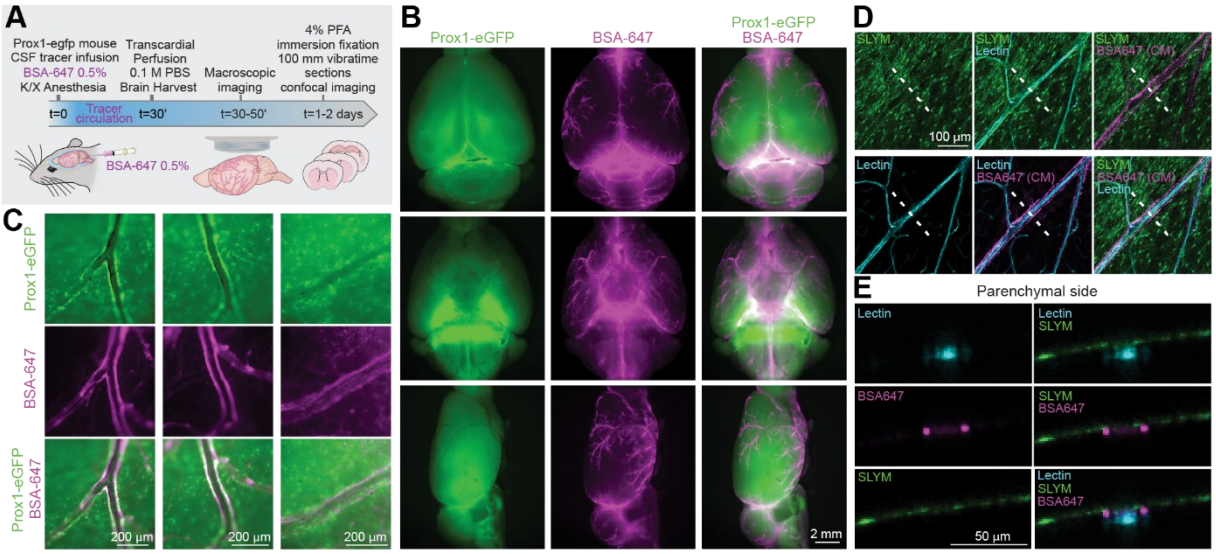

Supplementary Fig. 2: SLYM layer defines the perivascular space. (A) Scheme of the experimental approach. Tracer [BSA-647, 67 kDa, 0.5% (w/v), 10 µL, 2 µL/min] was delivered by cisterna magna cannulation to CSF space of K/X-anesthetized Prox1-eGFP mice. After 30 minutes circulation of the tracer, mice were perfused with PBS to eliminate blood vessel signal and brains were extracted and acutely imaged under a fluorescent microscope. **(B)** Macroscope fluorescent images of the whole brain, showing the basal cisterns filled with BSA-647 (magenta). Green signal corresponds to Prox1-eGFP expression. **(C)** Close-up images over the MCA at either the dorsal or ventral side illustrate the accumulation of BSA-647 in the periarterial space, covered by Prox1-eGFP+ cells. **(D)** Confocal Z-stacks confirmed the location of the fluorescent tracer in the perivascular space. Blood vessels were labelled internally with lectin (WGA-405, cyan) to improve the spatial location. **(E)** Reslicing of the confocal Z-stacks along the white line indicated in D showed the tridimensional distribution of the tracer (magenta) regarding SLYM (Prox1-eGFP+, green).